Receiver-Coordinated Distributed Transmit Nullforming with Channel State Uncertainty

D. Richard Brown III, Upamanyu Madhow, Patrick Bidigare, and Soura Dasgupta

Abstract—A distributed coherent transmission scheme in which two or more transmit nodes form a beam toward an intended receiver while directing nulls at a number of other "protected" receivers is considered. Unlike pure distributed beamforming, where the ith transmit coefficient depends only on the ith transmit node's channel to the intended receiver, the transmit coefficients of a distributed nullformer each depend on the channel responses from all of the transmit nodes to all of the protected nodes. The requirement for each transmit node to know all of the channels in the system makes distributed transmit nullforming challenging to implement in the presence of channel time variations. This paper describes a receivercoordinated distributed transmission protocol, in the context of a state-space dynamic channel model, in which the receive nodes feed back periodic channel measurements to the transmit cluster. The transmit nodes use this feedback to generate optimal channel predictions and then calculate a time-varying transmit vector that minimizes the average total power at the protected receivers while satisfying an average power constraint at the intended receiver during distributed transmission. We demonstrate via analysis and numerical simulation the efficacy of the technique even with low channel measurement overhead, infrequent update intervals, and significant feedback latency.

I. Introduction

We investigate the following canonical problem in cooperative communication: several transmit nodes sharing a common message form a beam towards an intended receiver while steering nulls toward a number of protected receivers. The *virtual array* formed by the transmission cluster is adapted to the propagation channels from each transmitter to each receiver, while accounting for the different timing references in the system. In this paper, we show that this can be accomplished effectively in a receiver-coordinated system, in which the channel coefficients from transmitters to receivers are predicted from explicit feedback provided by the receivers.

Transmit beamforming and nullforming are examples of *coherent* multi-input multi-output (MIMO) techniques, which require channel state knowledge at the transmitter (CSIT) at the transmitter. Such coherent schemes can provide compelling benefits over techniques that do not employ CSIT, as has been observed in the context of conventional MIMO schemes based on centralized antenna arrays [1]. However, realizing such

D.R. Brown III is an Associate Professor with the Electrical and Computer Engineering Department, Worcester Polytechnic Institute, Worcester, MA 01609 USA, e-mail: drb@ece.wpi.edu. U. Madhow is a Professor with Department of Electrical and Computer Engineering, University of California, Santa Barbara, CA 93106 USA, e-mail: madhow@ece.ucsb.edu. P. Bidigare is a Technology Director with BBN Technologies, Arlington, VA 22207 USA, email: bidigare@ieee.org. S. Dasgupta is a Professor with the Department of Electrical and Computer Engineering, University of Iowa, Iowa City, IA 52242 USA, e-mail: dasgupta@engineering.uiowa.edu.

coherent schemes in a distributed setting must address the additional challenge of synchronization across the cooperating transmitters, which in general do not have a common timing or carrier reference. Several techniques addressing this issue in the context of distributed transmit beamforming have emerged recently, with the goal of providing CSIT either implicitly or explicitly. These include receiver-coordinated explicit feedback [2]-[4], receiver-coordinated summarized feedback [5]-[7], master-slave synchronization with retrodirective transmission [8], round-trip retrodirective transmission [9], [10], and two-way synchronization with retrodirective transmission [11]. Each of these techniques has advantages and disadvantages in particular applications, as discussed in the survey article [12]. The significant recent progress on the subject of distributed transmit beamforming has even led to some preliminary experimental studies including [3], [6], [13].

Despite the recent progress on distributed transmit beamforming, all of the literature cited above considers a single intended receiver and does not account for the possibility of other receivers in the system that wish to be "protected" from the signals emitted by the distributed transmission cluster. In fact, since the distributed transmission cluster is typically a sparse array, sidelobes are often unavoidable in the transmit beam pattern and may lead to significant interference on unintended receivers [14]. This problem was considered in [15], [16] where a distributed "null-steering beamformer" was proposed such that the received power at unintended/protected receivers was set to zero while the received power at the intended receiver was maximized. The analysis in [15] assumes perfect synchronization of all of the nodes in the system and perfect "local" CSIT (i.e., each transmitter knows its own channel to all receivers, but not that of the other transmitters). Since a nullforming solution depends on the channels from all transmitters to all receivers, the focus of [15] is on approximate nullsteering based on local CSIT. Our metric for choosing beamsteering coefficients is similar to that in [15]: satisfy an average power constraint at an intended receiver (beamforming) while minimizing the total received power over a set of protected receivers (nullforming). Our approach, however, explicitly accounts for imperfect synchronization in tracking and predicting CSIT, and develops a solution that uses global CSIT predictions (i.e., we employ channel estimates between all transmitter-receiver pairs).

The key ingredient of our approach is the use of a state space model to capture the effects of stochastic clock drift and channel state uncertainty, using a receiver-coordinated protocol with explicit feedback. This approach was introduced for the purpose of distributed beamforming in [4], and we show here that it extends naturally to enable distributed nullforming as well. Clock drift and channel state uncertainty are particularly important for nullforming, since nulls tend to be less tolerant of channel estimation errors than beams. The analysis in this paper also accounts for feedback latency, which can lead to stale channel state predictions and degraded performance. Numerical results show that significant margins between intended and protected receiver power can be achieved in systems with low measurement overhead, relatively infrequent measurement intervals, and significant feedback latency.

II. SYSTEM MODEL

We consider the wireless communication system shown in Figure 1 with N transmit nodes, M protected receivers, and one intended receiver. For notational convenience, each node in the system is assumed to possess a single antenna. We also assume the transmit nodes have some mechanism by which they can share a common baseband message to be transmitted to the intended receiver and also have some rough level of synchronization so that they can effectively participate in the receiver-coordinated protocol schedule described in Section IV. The synchronization required here can be achieved with standard techniques such as global positioning system (GPS), network time protocol (NTP), or potentially through feedback messages from the receive nodes. Precise carrier synchronization as described in [11] is not assumed.

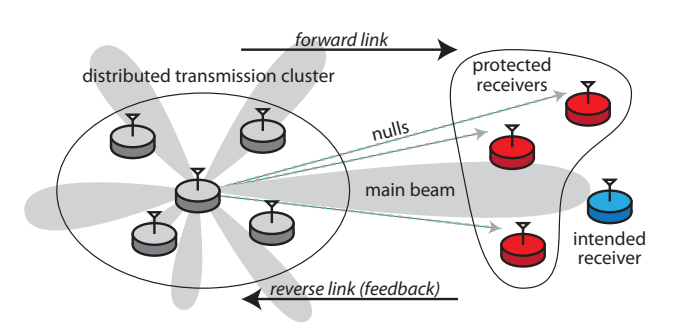


Fig. 1. System model with an N-node distributed transmission cluster, M protected receivers, and one intended receiver.

The nominal transmit frequency in the forward link from the distributed transmit cluster to the receivers is at ω_c . All forward link channels are modeled as narrowband, linear, and time invariant (LTI). Enumerating the protected receivers as $m=1,\ldots,M$ and adopting the convention that the intended receiver is node 0, we denote the channel from transmit node n to receive node m as $g^{(n,m)} \in \mathbb{C}$ for $n=1,\ldots,N$ and $m=0,\ldots,M$. These LTI propagation channels, in contrast to the time-varying "effective" channels described in the following sections, do not include the effect of carrier phase offsets between transmit node n and receive node m.

III. TWO-STATE OSCILLATOR MODEL

In conventional centralized antenna arrays, the array elements are driven by a common oscillator. An important distinction in distributed transmission schemes is that each transmit

node has an independent local oscillator. If the transmit nodes are not synchronized, the independent oscillators cause phase variations in each "effective" channel from transmit node n to receive node m even when the propagation channels $g^{(n,m)}$ are otherwise time invariant.

The carrier in a wireless transceiver is typically generated by multiplying up the frequency of a local oscillator. Based on the two-state local oscillator models in [17], [18], we define the discrete-time state of the $n^{\rm th}$ transmit node's carrier as $\boldsymbol{x}_t^{(n)}[k] = [\phi_t^{(n)}[k], \dot{\phi}_t^{(n)}[k]]^{\top}$ where $\phi_t^{(n)}[k]$ corresponds to the carrier phase offset in radians at transmit node n with respect to an ideal carrier phase reference at time k. The state update of the $n^{\rm th}$ transmit node's carrier is governed by

$$\boldsymbol{x}_{t}^{(n)}[k+1] = \boldsymbol{f}(T_s)\boldsymbol{x}_{t}^{(n)}[k] + \boldsymbol{u}_{t}^{(n)}[k]$$
 (1)

where the state update matrix

$$\mathbf{f}(T_s) = \begin{bmatrix} 1 & T_s \\ 0 & 1 \end{bmatrix},\tag{2}$$

and where T_s is an arbitrary sampling period selected to be short enough to avoid aliasing at the largest frequency offsets. The process noise vector $\boldsymbol{u}_t^{(n)}[k] \stackrel{\text{i.i.d.}}{\sim} \mathcal{N}\left(\mathbf{0}, \boldsymbol{Q}_t^{(n)}(T_s)\right)$ corresponds to the white frequency and random walk frequency process noises that cause the carrier derived from the local oscillator at transmit node n to deviate from an ideal linear phase trajectory. The covariance of the discrete-time process noise is derived from a continuous-time model in [17] and, in the context of carrier offsets, is given as

$$Q_t^{(n)}(T_s) = \omega_c^2 T_s \begin{bmatrix} p_t^{(n)} + q_t^{(n)} \frac{T_s^2}{3} & q_t^{(n)} \frac{T_s}{2} \\ q_t^{(n)} \frac{T_s}{2} & q_t^{(n)} \end{bmatrix}$$
(3)

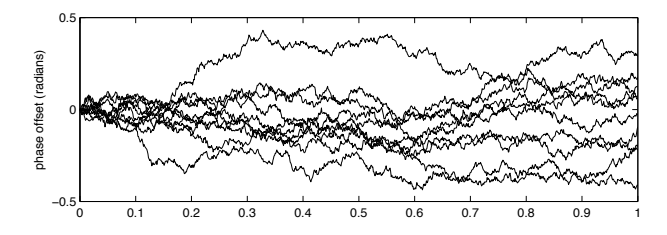
where ω_c is the nominal common carrier frequency in radians per second and $p_t^{(n)}$ (units of seconds) and $q_t^{(n)}$ (units of Hertz) are the process noise parameters corresponding to white frequency noise and random walk frequency noise, respectively. The process noise parameters $p_t^{(n)}$ and $q_t^{(n)}$ can be estimated by fitting the theoretical Allan variance

$$\sigma_y^2(\tau) = \frac{p_t^{(n)}}{\tau} + \frac{q_t^{(n)}\tau}{3} \tag{4}$$

to experimental measurements of the Allan variance for a particular family of oscillators over a range of τ values.

Figure 2 shows an example of ten independent state evolutions according to (1) with p_t and q_t parameters estimated from the Rakon RPFO45 oven-controlled oscillator datasheet and scaled for a carrier at 900 MHz. To isolate the effect of the process noise on the carriers, each state evolution was initialized at $\boldsymbol{x}_t^{(i)}[0] = [0,0]^{\text{T}}$, i.e. each carrier was synchronized in both phase and frequency to the reference at k=0. After one second, the standard deviations of the carrier phase offsets and carrier frequency offsets are approximately 0.27 radians and 0.047 radians/sec, respectively.

The receivers in the system shown in Figure 1 also have independent local oscillators used to generate carriers for downmixing that are governed by the same dynamics as (1) with state $\boldsymbol{x}_r^{(m)}[k]$, process noise $\boldsymbol{u}_r^{(m)}[k]$ $\stackrel{\text{i.i.d.}}{\sim} \mathcal{N}(0, \boldsymbol{Q}_r^{(m)}(T_s))$,



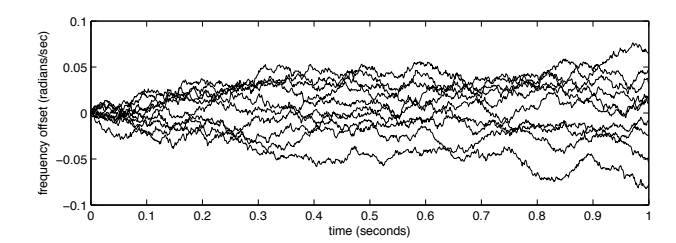


Fig. 2. Example oscillator dynamics showing ten independent state evolutions according to (1) with initial state $\mathbf{x}_t^{(i)}[0] = [0,0]^{\top}$.

and process noise parameters $p_r^{(m)}$ and $q_r^{(m)}$ as in (3) for $m=0,\ldots,M$. Transmissions from node n to receiver m are conveyed on a carrier nominally at ω_c generated at node n, incur a phase shift over the wireless channel $g^{(n,m)}$, and are then downmixed by receiver m using the local carrier nominally at ω_c at receiver m.

At time k, the "effective" channel from transmit node n to receive node m, including the carrier phase offset, can be written as

$$\begin{split} h^{(n,m)}[k] &= g^{(n,m)} e^{j\left(\phi_t^{(n)}[k] - \phi_r^{(m)}[k]\right)} \\ &= |g^{(n,m)}| e^{j\left(\phi_t^{(n)}[k] + \psi^{(n,m)} - \phi_r^{(m)}[k]\right)} \\ &= |g^{(n,m)}| e^{j\phi^{(n,m)}[k]} \end{split}$$

where $\psi^{(n,m)} = \angle g^{(n,m)}$ is the phase of the LTI channel from transmit node n to receiver m at the carrier frequency ω_c . In this context, we can define the *pairwise* carrier offset vector between transmit node n and receiver m as

$$\boldsymbol{\delta}^{(n,m)}[k] = \begin{bmatrix} \phi^{(n,m)}[k] \\ \dot{\phi}^{(n,m)}[k] \end{bmatrix} = \boldsymbol{x}_t^{(n)}[k] + \begin{bmatrix} \psi^{(n,m)} \\ 0 \end{bmatrix} - \boldsymbol{x}_r^{(m)}[k]. \tag{5}$$

The pairwise carrier offset is governed by the state update

$$\boldsymbol{\delta}^{(n,m)}[k+1] = \boldsymbol{f}(T_s)\boldsymbol{\delta}^{(n,m)}[k] + \boldsymbol{u}_{t}^{(n)}[k] - \boldsymbol{u}_{r}^{(m)}[k]$$
 (6)

where $f(T_s)$ is given in (2). At receiver m, the 2N-dimensional vector state of pairwise carrier offsets is then

$$egin{aligned} oldsymbol{\Delta}^{(m)}[k+1] &= egin{bmatrix} oldsymbol{\delta}^{(1,m)}[k+1] \ &dots \ oldsymbol{\delta}^{(N,m)}[k+1] \end{bmatrix} \ &= egin{bmatrix} oldsymbol{f}(T_s) \ &dots \ oldsymbol{f}(T_s) \end{bmatrix} oldsymbol{\Delta}^{(m)}[k] + egin{bmatrix} oldsymbol{u}_t^{(1)}[k] - oldsymbol{u}_r^{(m)}[k] \ &dots \ oldsymbol{u}_t^{(N)}[k] - oldsymbol{u}_r^{(m)}[k] \end{bmatrix} \ &= oldsymbol{F}(T_s) oldsymbol{\Delta}^{(m)}[k] + oldsymbol{z}^{(m)}[k]. \end{aligned}$$

Note $\boldsymbol{z}^{\scriptscriptstyle (m)}[k] = \boldsymbol{G}\boldsymbol{u}^{\scriptscriptstyle (m)}[k]$ where

$$oldsymbol{G} = egin{bmatrix} oldsymbol{I}_2 & & & -oldsymbol{I}_2 \ & \ddots & & dots \ & & oldsymbol{I}_2 & -oldsymbol{I}_2 \end{bmatrix} ext{ and } oldsymbol{u}^{(m)}[k] = egin{bmatrix} oldsymbol{u}^{(1)}_t[k] \ dots \ oldsymbol{u}^{(N)}_t[k] \ oldsymbol{u}^{(N)}_r[k] \end{bmatrix}$$

and where I_2 is the 2×2 identity matrix. Under the assumption that the constituent clock process noises are all independent such that $\operatorname{cov}\{\boldsymbol{u}^{(m)}[k]\} = \boldsymbol{Q}^{(m)}(T_s) = \operatorname{blockdiag}\{\boldsymbol{Q}_t^{(1)}(T_s),\dots,\boldsymbol{Q}_t^{(N)}(T_s),\boldsymbol{Q}_r^{(m)}(T_s)\},$ we can say the 2N-dimensional vector process noise at receiver m is distributed as $\boldsymbol{z}^{(m)}[k] \sim \mathcal{N}\left(\mathbf{0},\boldsymbol{G}\boldsymbol{Q}^{(m)}(T_s)\boldsymbol{G}^{\top}\right)$.

IV. RECEIVER-COORDINATED PROTOCOL

An overview of the receiver-coordinated distributed transmission protocol is shown in Figure 3. Forward transmissions are divided into measurement and beamforming epochs, repeating periodically with period T_s which corresponds to the measurement interval. Reverse link transmissions provide feedback from the receive nodes to the transmit nodes and are assumed to be on a different frequency than the uplink signals. Note that the protocol includes the effects of feedback latency since the feedback is typically not incorporated in the transmit weights until a later distributed transmission interval.

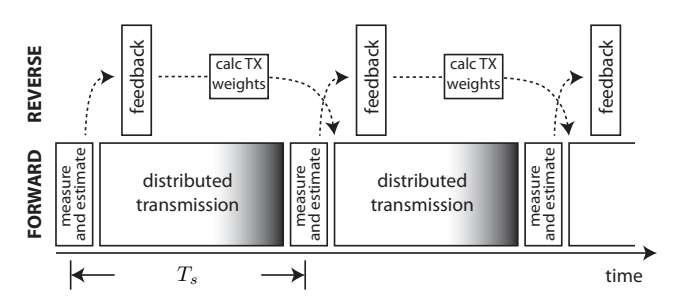


Fig. 3. Receiver-coordinated distributed transmission.

During the forward link measurement intervals, the transmit nodes simultaneously transmit using code division multiple access to facilitate signal separation at the receive nodes. We assume the duration of the measurement transmissions is small with respect to the frequency offsets such that the phase of the received signal is approximately constant during the measurement epoch. At time k, receive node m directly downmixes the received carrier from transmit node n with its own local carrier and estimates the resulting phase offset according to the observation model

$$\mathbf{y}^{(m)}[k] = \begin{bmatrix} 1 & 0 \\ & \ddots & \ddots \\ & & 1 & 0 \end{bmatrix} \mathbf{\Delta}^{(m)}[k] + \begin{bmatrix} v^{(1,m)}[k] \\ \vdots \\ v^{(N,m)}[k] \end{bmatrix}$$
(7)
$$= \mathbf{H} \mathbf{\Delta}^{(m)}[k] + \mathbf{v}^{(m)}[k]$$
(8)

where $\boldsymbol{v}^{(m)}[k] \overset{\text{i.i.d.}}{\sim} \mathcal{N}(0,\boldsymbol{R}^{(m)})$ is the additive white Gaussian measurement noise in the observation with $\boldsymbol{R}^{(m)} = \text{diag}(r^{(1,m)},\ldots,r^{(N,m)})$.

Since the pairwise offset states are coupled across receive nodes, the optimal approach to tracking the states is to feed the M+1 measurement vectors (8) back to the transmit nodes and have each transmit node apply the overall measurement vector to a Kalman filter to generate the joint MMSE state estimate $\hat{\Delta}[k\,|\,k] \in \mathbb{R}^{2N(M+1)}$. This approach, however, places the computational burden on the transmit nodes and also results in redundant computation. We propose instead a suboptimal (but more scalable) approach in which each receive node applies its observation vector $\mathbf{y}^{(m)}[k]$ to a local Kalman filter to generate a local MMSE state estimate $\hat{\Delta}^{(m)}[k\,|\,k] \in \mathbb{R}^{2N}$. These state estimates are then fed back to the transmit cluster to facilitate the calculation of the distributed transmit vectors.

Once the transmit cluster has received the feedback, the phase of the effective channels at any time $\ell > k$ can be straightforwardly predicted. Denoting the MMSE phase prediction as $\hat{\phi}^{(n,m)}[\ell \mid k]$, we can write the effective channel prediction from transmitter n to receiver m at time k as

$$\hat{h}^{(n,m)}[\ell \mid k] = |g^{(n,m)}|e^{j\hat{\phi}^{(n,m)}[\ell \mid k]}$$
(9)

since the channel amplitudes are assumed to be known. We denote the vector of channel predictions from all transmit nodes to receive node m as $\hat{\boldsymbol{h}}^{(m)}[\ell\,|\,k]\in\mathbb{C}^N$ for $\ell>k$. This vector of channel predictions can be extracted directly from the Kalman filter state prediction $\hat{\boldsymbol{\Delta}}^{(m)}[\ell\,|\,k]$ for any $\ell>k$.

Each transmit node performs the same calculations and, in the absence of feedback errors, generates the same effective channel predictions (9) and prediction error covariance matrices $\Sigma^{(m)}[\ell|k]$. These quantities are used to calculate the transmission vector $\boldsymbol{w}[\ell] \in \mathbb{C}^N$ such that the total expected interference power is minimized subject to the expected intended receiver power constraint. The details of how the transmission vector is calculated are discussed in the following section.

V. TRANSMISSION VECTOR CALCULATION

This section derives a closed-form expression for the transmit vector $\boldsymbol{w}[\ell] \in \mathbb{C}^N$ based on feedback from the receive nodes and the prediction error covariance matrices $\boldsymbol{\Sigma}^{(m)}[\ell|k]$. The n^{th} coefficient of the transmit vector $\boldsymbol{w}[\ell]$ specifies the transmit amplitude and phase of transmit node n at time ℓ . The goal is to select transmit coefficients such that a beam is formed toward the intended receiver and nulls are steered toward the protected receivers.

If M < N, one approach to forming a transmit vector is to select $\boldsymbol{w}[\ell]$ to be orthogonal to $\hat{\boldsymbol{h}}^{(m)}[\ell|k]$ for all $m=1,\ldots,M$ and then scale the resulting transmit vector to satisfy a power constraint. This "zero-forcing" transmit vector [16] effectively causes the total *predicted* instantaneous received power at the protected receive nodes to become zero. The *actual* instantaneous received power at the protected receive nodes will not be zero, of course, since the channel predictions are imperfect [16]. The zero-forcing approach also does not factor the uncertainty of the channel predictions into the calculation of the transmit vector. Intuitively, we would like an approach that optimally attenuates the transmissions of the nodes with less

certain channels to avoid the case of poor channel predictions "spoiling" the nulls.

Our approach here is to find a transmission vector $\boldsymbol{w}[\ell]$ that minimizes the total *expected* interference power subject to an *expected* power constraint at the intended receiver. By formulating the problem in terms of expected powers, the transmit vector calculation accounts for the uncertainty of the channel predictions. This formulation also effectively maximizes the ratio of the average power at the intended receiver to the average total interference power.

To develop an explicit method for calculating the transmit vector, we denote

$$oldsymbol{S}^{(m)}[\ell|k] = \mathrm{E}\left\{\hat{oldsymbol{h}}^{(m)}[\ell|k]\left(\hat{oldsymbol{h}}^{(m)}[\ell|k]
ight)^H
ight\} \in \mathbb{C}^{N imes N}$$

and state the optimization problem as

$$\mathbf{w}[\ell] = \arg\min_{\mathbf{v} \in \Gamma^{(0)}} \sum_{m=1}^{M} \mathbf{E} \left\{ \left| \mathbf{v}^{H} \hat{\mathbf{h}}^{(m)}[\ell|k] \right|^{2} \right\}$$

$$= \arg\min_{\mathbf{v} \in \Gamma^{(0)}} \mathbf{v}^{H} \left(\sum_{m=1}^{M} \mathbf{S}^{(m)}[\ell|k] \right) \mathbf{v}$$

$$= \arg\min_{\mathbf{v} \in \Gamma^{(0)}} \mathbf{v}^{H} \mathbf{A}[\ell|k] \mathbf{v}$$

where $\Gamma^{(0)} = \{ \boldsymbol{v} \in \mathbb{C}^N : \boldsymbol{v}^H \boldsymbol{S}^{(0)}[\ell|k] \boldsymbol{v} = \beta \}$. Since $\boldsymbol{A}[\ell|k]$ and $\boldsymbol{S}^{(0)}[\ell|k]$ are both Hermitian and positive definite, the solution to this optimization problem is well known [19, p.176] and is given as the eigenvector corresponding to the smallest eigenvalue in $\boldsymbol{B}[\ell|k] = \left(\boldsymbol{S}^{(0)}[\ell|k]\right)^{-1} \boldsymbol{A}[\ell|k]$, scaled to satisfy the constraint $\boldsymbol{v}^H \boldsymbol{S}^{(0)}[\ell|k] \boldsymbol{v} = \beta$.

We focus now on developing an explicit expression for $S^{(m)}[\ell|k]$ in terms of the known quantities at each transmit node. First, we write the effective channel prediction in (9) as

$$\hat{h}^{(n,m)}[\ell|k] = |g^{(n,m)}|e^{j\left(\phi^{(n,m)}[\ell|k] + \tilde{\phi}^{(n,m)}[\ell|k]\right)}$$
(10)

where $\tilde{\phi}^{(n,m)}[\ell|k]$ represents the prediction error of the channel phase. We can then write the $(i,n)^{\text{th}}$ element of $S^{(m)}[\ell|k]$ as

$$\begin{split} \boldsymbol{S}_{i,n}^{(m)}[\ell|k] &= |g^{(i,m)}||g^{(n,m)}|e^{j(\phi^{(i,m)}[\ell|k] - \phi^{(n,m)}[\ell|k])} \times \\ &\quad \mathbb{E}\left\{e^{j(\tilde{\phi}^{(i,m)}[\ell|k] - \tilde{\phi}^{(n,m)}[\ell|k])}\right\}. \end{split}$$

To evaluate the expectation, we assume the phase prediction errors are small such that the Taylor series approximations

$$\begin{split} & \sin(\tilde{\phi}^{(i,m)}[\ell|k] - \tilde{\phi}^{(n,m)}[\ell|k]) \approx \tilde{\phi}^{(i,m)}[\ell|k] - \tilde{\phi}^{(n,m)}[\ell|k], \\ & \cos(\tilde{\phi}^{(i,m)}[\ell|k] - \tilde{\phi}^{(n,m)}[\ell|k]) \approx 1 - \frac{(\tilde{\phi}^{(i,m)}[\ell|k] - \tilde{\phi}^{(n,m)}[\ell|k])^2}{2} \end{split}$$

hold. Then we can write

$$\begin{split} \mathbf{E} \left\{ e^{j(\tilde{\phi}^{(i,m)}[\ell|k] - \tilde{\phi}^{(n,m)}[\ell|k])} \right\} &\approx 1 - \frac{\mathbf{E} \left\{ (\tilde{\phi}^{(i,m)}[\ell|k] - \tilde{\phi}^{(n,m)}[\ell|k])^2 \right\}}{2} \\ &= 1 - \frac{\sigma_{i,m}^2[\ell|k] - 2\rho_{i,n,m}[\ell|k] + \sigma_{n,m}^2[\ell|k]}{2} = \xi_{i,n}^{(m)}[\ell|k] \end{split}$$

where $\sigma_{i,m}^2[\ell|k]$ is the prediction variance of the phase offset from transmit node i to receive node m at time k, $\sigma_{n,m}^2[\ell|k]$ is the same except from transmit node n, and $\rho_{i,n,m}[\ell|k]$ is

the prediction covariance. Note that $\rho_{i,n,m}[\ell|k] \neq 0$ because the receiver's clock drift is a common source of error for both phase predictions. Also note that these quantities are all elements of the prediction covariance matrix $\Sigma^{(m)}[\ell|k]$.

Finally, under our small angle assumption, we can write

$$e^{j(\phi^{(i,m)}[k] - \phi^{(n,m)}[k])} \approx e^{j(\hat{\phi}^{(i,m)}[k] - \hat{\phi}^{(n,m)}[k])}$$
 (11)

where these pairwise phase offset predictions can be extracted from the state prediction vector $\hat{\boldsymbol{\Delta}}^{(m)}[\ell|k]$. Putting this all together, the $(i,n)^{\text{th}}$ element of $\boldsymbol{S}^{(m)}[\ell|k]$ is approximated as

$$\boldsymbol{S}_{i,n}^{(m)}[\ell|k] \approx \begin{cases} |g^{(i,m)}|^2 & i = n \\ |g^{(i,m)}||g^{(n,m)}|e^{j(\hat{\phi}^{(i,m)}[\ell|k] - \hat{\phi}^{(n,m)}[\ell|k])} \xi_{i,n}^{(m)}[\ell|k] & i \neq n. \end{cases}$$

All of these quantities are identically computed at the transmit nodes based on the feedback from the receive nodes. Hence, the transmit nodes can arrive at a common transmit vector $\boldsymbol{w}[\ell]$ at any point in a transmission epoch, from which each transmit node extracts its transmit coefficient to adjust its local carrier phase and amplitude. Note these transmit coefficients are not used during measurement epochs.

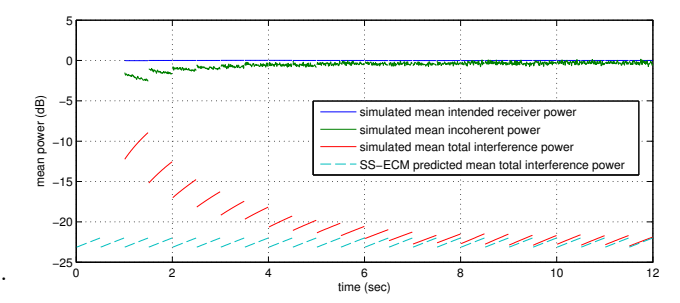
VI. NUMERICAL RESULTS

This section presents two numerical examples of the receiver-coordinated distributed nullforming technique described in this paper. In both examples, N=4 transmit nodes were randomly placed on a disk with diameter 5 meters centered at the origin. The intended receive node was placed at (x, y) coordinates (50,0) and M = 2 protected receive nodes were placed at $(50\cos(\pi/8), 50\sin(\pi/8))$ and $(50\cos(-\pi/8), 50\sin(-\pi/8))$ with all units in meters. The received power constraint at the intended receive node was set to $\beta = 1$. The carrier frequency was set to $f_c = 900$ MHz and the protocol used a measurement interval of $T_s = 0.5$ seconds. The measurement epoch was set to the first 10 ms of each 500 ms measurement interval, corresponding to a 2% measurement overhead. The feedback latency was set to one full measurement interval, i.e. measurements are not incorporated in the Kalman filter predictions of the immediately subsequent distributed transmission interval (as illustrated in Figure 3).

In each iteration of the Monte Carlo simulations, new realizations of the transmit node positions, initial frequency offsets, clock process noises, and measurement noises were generated. The oscillators' initial frequency offsets were uniformly distributed over ± 0.04 ppm, which corresponds to ± 36 Hz at a nominal carrier frequency of 900 MHz. A single-path propagation model was assumed with channel amplitudes calculated as $|g^{(n,m)}|=\frac{50}{d^{(n,m)}}$ where $d^{(n,m)}$ is the distance between transmit node n and receive mode m in meters. The nominal phase offset measurement noise variance was set to $r^{(n,m)}=\frac{((5/360)2\pi)^2}{|g^{(n,m)}|}$ which corresponds to a standard deviation of 5 degrees at a range of 50 meters.

Figure 4 shows the results of a Monte-Carlo simulation with homogeneous process noise parameters: $p_t^{(n)} = p_r^{(m)} = 3 \times 10^{-4}$ and $q_t^{(n)} = q_r^{(m)} = 1 \times 10^{-2}$ for all $n=1,\ldots,N$ and $m=0,\ldots,M$. Distributed transmission begins at t=1.010 seconds, corresponding to the start of the first distributed

transmission epoch in which the Kalman filter phase predictions were accurate enough to ensure the small angle approximations used in Section V were reasonable.



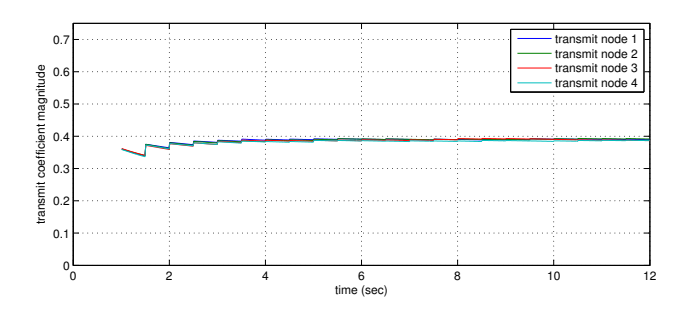


Fig. 4. Received power simulation homogeneous process noise parameters.

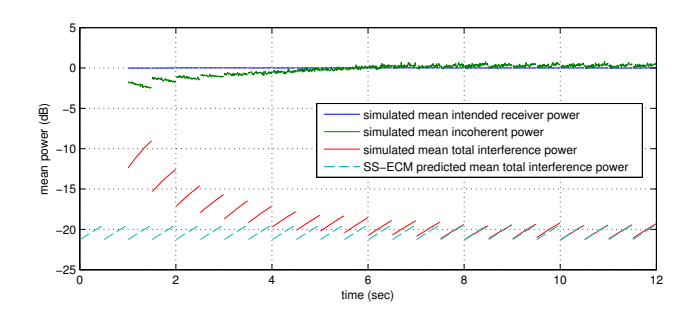
These results show that, initially, when the channel predictions are relatively inaccurate, the transmit coefficients prioritize beamforming, as can be seen in the initial gap between the mean intended receiver power and the mean incoherent power. As the channel predictions become more accurate, the optimal transmit vector prioritizes nullforming and, in this example, the mean intended receiver power is only slightly above the mean incoherent power. These results also show that the transmit coefficient magnitudes tend to be smaller when the channel predictions are less accurate.

After the initial transient, the average total interference power settles into a steady-state range between approximately $-22~\mathrm{dB}$ and $-23~\mathrm{dB}$, demonstrating that effective nulls are being driven toward the protected receivers. The nulling performance is better at the start of each distributed transmission interval but degrades somewhat by the end of the distributed transmission interval as the state predictions become more stale. This can be ameliorated to some extent by shortening the measurement interval and/or reducing the feedback latency.

Since the process and measurement noises are homogeneous in this example, all of the transmit nodes have identical average transmit coefficient magnitudes. Figure 5 shows the results of a Monte-Carlo simulation with *heterogeneous* process noise parameters: $p_t^{(1)} = 3 \times 10^{-3}$ and $q_t^{(1)} = 1 \times 10^{-1}$; all other process noise parameters unchanged. In other words, transmit node 1 now has a less stable oscillator than all of the other nodes in the system.

After the initial transient, Figure 5 shows the average total interference power settles into a periodic steady-state range between approximately -19.5 dB and -21 dB, which is

slightly worse than the homogeneous process noise parameter simulation in Figure 4. We also see that transmit node 1's average transmit coefficient magnitude is reduced with respect to the remaining three transmit nodes with more stable oscillators. This demonstrates that the transmit vector calculation accounts for state prediction uncertainty by emphasizing the more predictable transmit nodes and deemphasizing the transmit node with the less stable oscillator.



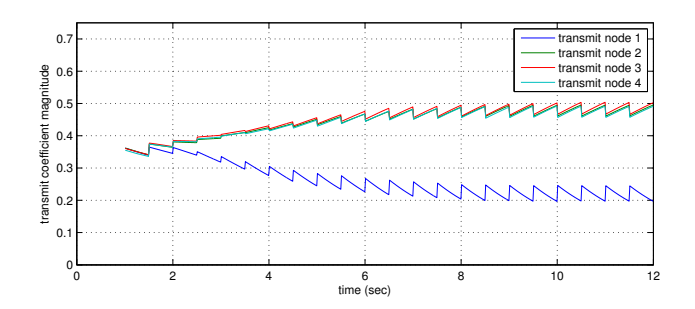


Fig. 5. Received power simulation heterogeneous process noise parameters.

Finally, the dashed cyan line in both results represents the predicted performance based on a steady-state error covariance analysis of the system. This involves determining the prediction error covariance $\mathbf{\Sigma}^{(m)}[k_0+k\,|\,k]$ as $k\to\infty$ by solving a discrete-time algebraic Riccati equation [20] and projecting the prediction covariances through the distributed transmission epoch. In both cases we see that, after the initial transient, which lasts about 10 seconds, the Monte-Carlo simulations agree closely with the steady-state predictions.

VII. CONCLUSION

The method presented here allows the formation of a beam towards an intended receiver, while steering nulls at protected receivers. Nullforming is more sensitive than beamforming to errors in channel state, and to the best of our knowledge, this is the first paper to show that it can be achieved effectively in a distributed setting despite stochastic clock dynamics. Our numerical results show that significant margins between intended and protected receiver power can be achieved in systems with low measurement overhead, relatively infrequent measurement intervals, and significant feedback latency. An important topic for future work is to investigate the effect of loss or corruption of the feedback information. It is also important to study the impact of peak power constraints: a standard null-steering solution has significant amplitude

variations across transmit nodes, and it is of interest to see if it is possible to obtain good beam-to-null powers under a peak-to-average power variation constraint across transmitters.

REFERENCES

- A. Scaglione, P. Stoica, S. Barbarossa, G. Giannakis, and H. Sampath, "Optimal designs for space-time linear precoders and decoders," Signal Proc., IEEE Transactions on, vol. 50, no. 5, pp. 1051–1064, May 2002.
- [2] Y. Tu and G. Pottie, "Coherent cooperative transmission from multiple adjacent antennas to a distant stationary antenna through AWGN channels," in *IEEE Vehicular Technology Conf. (VTC)*, vol. 1, Birmingham, AL, Spring 2002, pp. 130–134.
- [3] R. Irmer, H. Droste, P. Marsch, M. Grieger, G. Fettweis, S. Brueck, H.-P. Mayer, L. Thiele, and V. Jungnickel, "Coordinated multipoint: Concepts, performance, and field trial results," *Communications Magazine, IEEE*, vol. 49, no. 2, pp. 102–111, Feb. 2011.
- [4] D.R. Brown III, P. Bidigare, and U. Madhow, "Receiver-coordinated distributed transmit beamforming with kinematic tracking," in *Proceedings of the 37th International Conference on Acoustics, Speech, and Signal Processing (ICASSP)*, 2012, accepted to appear.
- [5] R. Mudumbai, J. Hespanha, U. Madhow, and G. Barriac, "Scalable feedback control for distributed beamforming in sensor networks," in *IEEE International Symp. on Information Theory (ISIT)*, Adelaide, Australia, September 2005, pp. 137–141.
- [6] R. Mudumbai, B. Wild, U. Madhow, and K. Ramchandran, "Distributed beamforming using 1 bit feedback: from concept to realization," in 44th Allerton Conf. on Comm., Control, and Computing, Monticello, IL, Sep. 2006, pp. 1020 – 1027.
- [7] R. Mudumbai, J. Hespanha, U. Madhow, and G. Barriac, "Distributed transmit beamforming using feedback control," *IEEE Trans. on Information Theory*, vol. 56, no. 1, pp. 411–426, January 2010.
- [8] R. Mudumbai, G. Barriac, and U. Madhow, "On the feasibility of distributed beamforming in wireless networks," *IEEE Trans. on Wireless Communications*, vol. 6, no. 5, pp. 1754–1763, May 2007.
- [9] I. Ozil and D.R. Brown III, "Time-slotted round-trip carrier synchronization," in *Proc. of the 41st Asilomar Conf. on Signals, Systems, and Computers*, Pacific Grove, CA, November 4-7, 2007, pp. 1781 – 1785.
- [10] D.R. Brown III and H.V. Poor, "Time-slotted round-trip carrier synchronization for distributed beamforming," *IEEE Trans. on Signal Process*ing, vol. 56, no. 11, pp. 5630–5643, November 2008.
- [11] R. Preuss and D.R. Brown III, "Two-way synchronization for coordinated multi-cell retrodirective downlink beamforming," *IEEE Trans. Signal Proc.*, vol. 59, no. 11, pp. 5415–27, Nov. 2011.
- [12] R. Mudumbai, D.R. Brown III, U. Madhow, and H.V. Poor, "Distributed transmit beamforming: Challenges and recent progress," *IEEE Commu*nications Magazine, vol. 47, no. 2, pp. 102–110, February 2009.
- [13] D. Brown, B. Zhang, B. Svirchuk, and M. Ni, "An experimental study of acoustic distributed beamforming using round-trip carrier synchronization," in *Phased Array Systems and Technology (ARRAY)*, 2010 IEEE International Symposium on, Oct. 2010, pp. 316 –323.
- [14] H. Ochiai, P. Mitran, H.V. Poor, and V. Tarokh, "Collaborative beamforming for distributed wireless ad hoc sensor networks," *IEEE Trans.* on Signal Processing, vol. 53, no. 11, pp. 4110 – 4124, November 2005.
- [15] K. Zarifi, S. Affes, and A. Ghrayeb, "Collaborative null-steering beamforming for uniformly distributed wireless sensor networks," *IEEE Trans. on Signal Proc.*, vol. 58, no. 3, pp. 1889 –1903, March 2010.
- [16] D.R. Brown III, P. Bidigare, S. Dasgupta, and U. Madhow, "Receiver-coordinated zero-forcing distributed transmit nullforming," in *IEEE Statistical Signal Processing Workshop*, 2012, in review.
- [17] L. Galleani, "A tutorial on the two-state model of the atomic clock noise," *Metrologia*, vol. 45, no. 6, pp. S175–S182, December 2008.
- [18] G. Giorgi and C. Narduzzi, "Performance analysis of kalman filter-based clock synchronization in IEEE 1588 networks," in *International IEEE Symposium on Precision Clock Synchronization for Measurement, Control, and Communication*, October 12-16 2009, pp. 1–6.
- [19] R. Horn and C. Johnson, *Matrix Analysis*. New York, NY: Cambridge University Press, 1994.
- [20] Y. Bar-Shalom, X. R. Li, and T. Kirubarajan, Estimation with Applications to Tracking and Navigation. John Wiley and Sons, 2001.